HHS Public Access

Author manuscript

Photochem Photobiol. Author manuscript; available in PMC 2022 March 01.

Published in final edited form as:

Photochem Photobiol. 2021 March ; 97(2): 416–426. doi:10.1111/php.13339.

Photo-destruction of Stromal Fibroblasts Enhances Tumor Response to PDT in 3D Pancreatic Cancer Co-culture Models

Vida Karimnia[1], **Imran Rizvi**[2,3], **Frank J. Slack**[4], **Jonathan P. Celli**[*,1]

[1]Department of Physics, University of Massachusetts at Boston, Boston, MA, 02125, USA

[2]Joint Department of Biomedical Engineering, University of North Carolina at Chapel Hill, Chapel Hill, NC and North Carolina State University, Raleigh, NC, 27599, USA

[3]Lineberger Comprehensive Cancer Center, University of North Carolina School of Medicine, Chapel Hill, NC, 27599, USA

[4]Department of Pathology, BIDMC Cancer Center/Harvard Medical School; 330 Brookline Avenue, Boston, MA, 02215, USA

Abstract

Pancreatic ductal adenocarcinoma (PDAC) is among the most lethal of human cancers. The dismal response of PDAC to virtually all therapeutics is associated, in part, with a characteristically dense fibrotic stroma. This stroma acts not only as a barrier to drug perfusion, but also promotes tumor survival through paracrine crosstalk and biophysical interactions. Photodynamic therapy (PDT) is being explored for PDAC treatment, though the impact of tumor-promoting stromal crosstalk on PDT response in PDAC is not well characterized. The current study assesses the effect of tumor-stroma interactions on response to PDT or chemotherapy in heterocellular 3D co-cultures using PDAC cells and two different fibroblastic cell types (pancreatic stellate cells, PSCs, and a normal human fibroblast cell line, MRC5) embedded in extracellular matrix (ECM). While stromal fibroblasts promote resistance to chemotherapy as expected, PDAC 3D nodules in co-culture with fibroblasts exhibit increased response to PDT relative to homotypic cultures. These results point to the potential for PDT to overcome tumor-promoting stromal interactions associated with poor therapeutic response in PDAC.

Introduction:

Pancreatic ductal adenocarcinoma (PDAC) has one of the lowest survival rates of all cancers, and few therapeutic options. Less than one quarter of patients have resectable tumors while chemotherapy is generally palliative and often not well-tolerated (1). Histologically, PDAC is characterized by a prominent desmoplastic reaction surrounding malignant epithelial cells, which is associated with therapeutic resistance (2) (3) (4) (5). The dense fibrotic PDAC stroma consists largely of pancreatic stellate cells (PSCs) with abundant extracellular matrix (ECM) rich in collagen, fibronectin, laminin, and elastin (6). PSCs remain in a quiescent state in normal pancreas but become activated during pancreatic

*Corresponding author's Jonathan.Celli@umb.edu (Jonathan P. Celli).

injury. As the injury resolves, the secreted matrix metalloproteinases (MMPs) degrade the excess fibrosis (2). However, during PDAC, the imbalance between ECM production and degradation results in dense fibrotic stroma produced by activated PSCs (7). The ECM compresses blood vessels, and, as a result, reduces perfusion and increases hypoxia and blood pressure, thereby decreasing drug delivery. The complexity of stromal cross talk is increased by its inherent heterogeneity. A recent study by Biffi *et al.* identified two distinct cancer-associated fibroblast (CAF) subtypes characterized with myofibroblastic (myCAF) or inflammatory (iCAF) phenotypes (8). MyCAFs are in direct contact with tumor cells and restrain tumor progression through juxtacrine signaling. In contrast, iCAFs are more distant from the tumor cells within the dense stroma and exhibit an inflammatory phenotype. In tumor organoids, iCAFs are shown to activate pathways that are important for proliferation and survival.

While the prominent role of PDAC stroma in therapeutic resistance has motivated the development of stromal depletion therapies, this approach has had mixed results. Among the early approaches was to therapeutically target CAFs to enhance response to chemotherapy (9) (10) (11) (12) (13). Anti-CAF therapies initially showed promise, though later studies showed that the situation may be more complex and depletion of stroma can in fact result in more aggressive tumor growth. Sonic hedgehog (Shh) signaling emerged as a key contributor to development of PDAC desmoplasia and a potential therapeutic target (14). Preclinical evaluation of Shh pathway inhibition appeared to be a promising strategy in PDAC mouse models, which exhibited depletion of stroma, increased microvessel density and enhanced response to chemotherapy (15). Notwithstanding promising preclinical results this approach failed in the clinic and a later study showed that Shh inhibition actually leads to acceleration of PDAC progression (16). In another preclinical study, a PDAC mouse model with depleted αSMA^+ myofibroblasts in PDAC led to enhanced epithelial mesenchymal transition (EMT) and invasion, and decreased survival (17). On the other hand, the promising results using abraxane for targeting CAFs in breast cancer suggest that this approach could be worth revisiting in targeted groups of patients with highly desmoplastic, fibroblast-rich tumors (18). Overall these studies show that stromal depletion is a complicated strategy, and that a balanced approach that considers both tumor suppressing and tumor promoting roles of the stroma is important to avoiding negative results.

Disappointing response of PDAC to both non-targeted and targeted therapies has motivated the investigation of photodynamic therapy (PDT). PDT is a photochemistry-based treatment modality that involves electronic excitation of a photosensitizer (PS) by an appropriate (usually red) light source to initiate the generation of reactive oxygen species in the target tissue (19) (20) (21) (22). Early studies demonstrated the promise of PDT in preclinical PDAC models (23), while more recent clinical studies have successfully established the technical feasibility and safety of PDT for locally advanced PDAC (24) (25). It has been shown that PDT is able to overcome chemoresistance (26) (27) (28). Moreover, PDT as a neoadjuvant treatment for disseminated pancreatic cancer has shown promise (29). Photodynamic priming (PDP) is a technique in which the light based production of reactive molecular species doesn’t surpass the cytotoxic threshold. It has been shown that PDP combined with vitamin D3 receptor activation in the tumor microenvironment overcomes

chemoresistance in PDAC by modulating a number of chemokines, and allows lower chemotherapy doses while maintaining significant and lasting treatment response (30). However, the role of stromal crosstalk specifically as a determinant of PDT response to PDAC has not been extensively studied. Previous studies in an in vitro 3D pancreatic tumor and fibroblast co-culture model showed that while PDT was able to destroy fibroblasts, it was unclear how this influenced tumor response to PDT and whether phenotypic traits of the fibroblasts were important to either the fibroblasts or tumor response to PDT (31). Another recent study examined the effect of PDT on pancreatic cancer cells co-cultured with fibroblasts in monolayer using semi-permeable inserts (32). This study showed that PDAC cell death in the presence of activated fibroblasts in monolayer was lower than the cell death in the presence of non-activated fibroblasts, though the difference was not statistically significant.

In this study, we adopted a heterotypic 3D co-culture model, which allowed us to examine PDT response of PDAC cells in communication with stromal partners that recapitulate contrasting fibroblastic phenotypes (33). While sophisticated animal models have been developed to recapitulate PDAC stroma (34) the use of a custom in vitro model here allowed us to interrogate response to PDT when epithelial PDAC cells are allowed to interact with stromal cells exhibiting contrasting fibroblastic phenotypes in a controlled environment that restores key morphological and functional features of human disease (2) (35).In this context we specifically examined how co-cultures with either primary pancreatic stellate cells (PSCs) or MRC5 cells (an established human fibroblast cell line), impacted upon growth, chemoresistance, and response to veteporfin PDT in PDAC 3D cultures. Co-cultures with each fibroblastic cell type were prepared using two epithelial PDAC lines, PANC-1 and CFPAC-1 cells to examine response with quasi mesenchymal and classical PDAC subtypes respectively (36). The formation of 3D multicellular PDAC nodules over a bed of stromal cells embedded in ECM enabled tumor-stroma paracrine crosstalk while allowing separate interrogation of therapeutic response in each population (in separate focal planes). We use this platform to contrast response to verteporfin PDT with two classical chemotherapy drugs with contrasting mechanisms of action: gemcitabine, a nucleoside analog; and oxaliplatin, an alkylating-like agent that is the major cytotoxic component of the multi-drug cocktail FOLFIRINOX.

Materials and Methods:

Cell culture:

PANC-1, CFPAC-1, and MRC5 cell lines were obtained from the ATCC and grown in T75 cell culture flasks according to ATCC guidelines. DMEM, IMDM and MEM (HyClone) were supplemented with 10% FBS (HyClone), 100 IU/mL penicillin and 1% streptomycin (HyClone), and 0.5 mg/mL Amphotericin B (Corning). PSC cell line was obtained from ScienCell. SteCM was supplemented with 1% SteCGS, 2% FBS and 1% penicillin. PSC and MRC5 cells were subcultured between 3-10 times before they were used in the experiment.

3D cell cultures and co-cultures:

PSC and MRC5 cells in single cell suspension were diluted to 100,000 cells in 250μl Growth factor reduced (GFR) Matrigel (240 mL; Corning) and added to each well of 24-well black-walled plate (Ibidi USA Inc.) and incubated at 37°C for 20 minutes to allow for gelation. The Matrigel beds were overlaid with single-cell suspensions of PANC-1, and CFPAC-1 cell lines at a concentration of 7,500 cells/mL in DMEM high glucose and IMDM respectively following standard procedure for Matrigel-based overlay 3D tumor models (37). Cultures were incubated at 37°C and fresh cultures which supplemented with 2% Matrigel were substituted with the original medium every two days. The nodule growth was monitored every other day via darkfield microscopy with 5x objective to obtain high contrast images (33). Longitudinal images were processed to obtain growth curves and size distribution data using analysis code that was previously described (38).

PDT treatments in 3D cultures:

PDT treatments were administered to 3D cultures 7 days after plating. Growth medium was substituted with medium containing 250 nmol/L verteporfin (benzoporphyrin derivative monoacid ring A, BPD) (Sigma-Aldrich), incubated at 37°C for 1 hour and then replaced with the original medium and irradiated with 690 nm laser source (Intense; New Brunswick,NJ). Total light dose ranged from 5 J/Cm^2 to 20 J/Cm^2 with irradiance of 100 mW/Cm^2 at the bottom surface of cell culture. In cases where treatment response was studied in monolayer cell cultures, PDT parameters were identical, but cultures were prepared in black-walled 96-well plates. Therapeutic response was analyzed using fluorescence imaging after 24 hours.

Chemotherapy treatments in 3D cultures:

Chemotherapy treatments were administered 7 days after plating cultures. For gemcitabine treatments culture wells were assigned to groups that received either fresh medium (no treatment control), 10 μM, 100 μM, or 1000 μM gemcitabine (Tocris; Bristol, UK). For oxaliplatin treatments culture wells were assigned to groups that received either fresh medium (no treatment control), 10 μM, 100 μM, or 500 μM oxaliplatin. Chemotherapy treatment response was assessed by fluorescence imaging and image analysis procedures as described below

Imaging-based analysis of treatment response:

Therapeutic response was analyzed using fluorescence imaging after 24 hours. The vital dyes calcein AM and Ethidium Bromide were used as fluorescent markers for live and dead cells respectively, and returned to the incubator for 40 minutes prior to imaging (27).Complete sets of image data were acquired for two different focal planes: An upper plane image with 3D tumor nodules in focus, and a lower position focal plane with the embedded fibroblasts tumor nodules. This 3D model geometry allows us to interrogate and analyze response in each cell population separately. The geometry of the model system is shown schematically in Figure 1. Treatment response was quantified from fluorescence image data using an adaptation of routines previously developed in MATLAB (Mathworks, Natick, MA) (39) (27). Briefly improvised, response was reported as the ratio of total viable

volume from summing over all nodules in each segmented calcein channel image to the viable volume of the respective no treatment control. The volume of interior dead (ethidium-bromide positive) segmented regions were subtracted from each nodule volume before summation.

Apoptosis and necrosis staining:

For imaging of apoptosis and necrosis, 3 hours after PDT, cultures were washed once with 1X annexin V binding buffer (Annexin V-FTTC Fluorescence Microscopy Kit, BD Biosciences; San Jose, CA) diluted from 10X stock using hypure™ cell culture grade water. The plates were incubated for 30 minutes in room temperature with annexin V (BD Biosciences; San Jose, CA), propidium iodide (BD Biosciences; San Jose, CA) and Hoechst (33342, Trihydrochloride, Trihydrate, ThermoFisher Scientific; Waltham, MA). Before taking images, this medium was replaced with 1X annexin V binding buffer for better resolution.

Immunofluorescence:

Cultures for immunofluorescence imaging were grown for 7 days, rinsed with DPBS then fixed with 4% formaldehyde, for 15 min. The formaldehyde was gently removed and the cells were permeabilized with 0.5% triton for 30 min. Next, the cells were quenched with 0.1M Glycine for 5 min. This step was repeated two more times. 50μl blocking buffer was added and the plate was stored at room temperature for 1 hour. Next, they were incubated with mouse anti-α-smooth muscle actine (α-SMA) and rabbit anti IL-1-α antibodies (Abcam, Cambridge, MA) overnight at 4°C. Next, they were rinsed with DPBS for 5 min three times followed by adding diluted goat anti-mouse IgG (α-SMA) and goat anti-rabbit IgG (IL-1-α) stored at 4°C for two hours. They were rinsed with DPBS and covered with prolong™ Diamond Antifade Mountant with DAPI (Thermo Fisher Scientific). The images were taken using both widefield and confocal microscopes with 40x and 20x objectives respectively.

Transforming growth factor-β (TGFβ) treatments

To examine response to TGFβ stimulation, 10 ng/mL TGFβ (Gibco, Thermo-Fisher Scientific; Frederick, MD) in 1% FBS DMEM was added to MRC5 and PSC cells in monolayer for 24 hours then stained for immunofluorescence as described above.

Results and Discussion:

MRC5 and PSC cells exhibit contrasting fibroblastic phenotypes in co-cultures with PANC-1 and CFPAC-1 PDAC cell lines

We performed immunofluorescence imaging experiments to evaluate relevant phenotypic traits in stromal and epithelial PDAC cells in co-culture. It has been shown that IL1-α signaling is associated with the iCAF phenotype, which is implicated in tumor-promoting behavior. The expression of α-SMA is consistent with the myCAF phenotype, which has been associated with a tumor suppressive role (8). A distinct difference in α-SMA and IL1-α expression was observed between PSC and MRC5 cells. As shown in Figures 2A and 2B, MRC5 had a higher IL1-α /α-SMA signal than PSC cells in both co-culture types (IL1-α

and α-SMA expressions in MRC5 and PCS cells co-cultured with PANC-1 or CFPAC-1 nodules in supplementary Figure 1). It has been shown that, depending on the tumor-derived cues the fibroblasts are exposed to, iCAFs and myCAFS are interconvertible (8). The contrasting fibroblast phenotypes observed in our results when co-cultured with different PDAC cells, PANC-1 and CFPAC-1 was presumably due to different tumor-derived cues to the fibroblasts from each of these PDAC cells. The results from RNA sequencing of a panel of 2D human PDAC lines show IL1-α expression is approximately 140 times higher in CFPAC-1 cells compared to PANC-1 cells ($P>0.05$). Also, α-SMA secretion is approximately 8 times higher in CFPAC-1 cells compared to PANC-1 cells ($P>0.05$) (40). This might be the reason that overall we observed more α-SMA and IL1-α signaling in both types of fibroblasts when co-cultured with CFPAC-1 compared to when co-cultured with PANC-1. Overall, our data showed that the PSCs and MRC5 cells had different phenotypes when co-cultured with different PDAC cells. Whether these phenotypic differences could affect tumor growth and response to PDT and chemotherapy was investigated.

Comparative analysis of growth behavior in homotypic and co-culture

Having identified PDAC-relevant contrasting phenotypic traits of PCSs and MRC5 cells in co-culture, we sought to further probe the overall growth behavior of PDAC 3D cultures with and without each fibroblastic cell type in co-culture. These experiments used darkfield microscopy imaging at multiple timepoints to establish growth curves and to study the evolution of nodule size distribution over time (Figure 3). The results for both PANC-1 and CFPAC-1 cells were consistent with the expectation that the number of multicellular 3D nodules decreases due to cell and nodule aggregation events, while the size of nodules increases due to both aggregation and proliferation at the same time, as reported previously for other cancer cell lines in ECM overlay 3D culture (38). As Figure 3C shows, PANC-1 nodule size increased more rapidly in the presence of PSCs. To examine the relative roles of proliferation or aggregation in nodule size increase, the number of nodules per day for each condition was also reported. Figure 3C shows, the number of PANC-1 nodules decreased with the same amount in all conditions (+/−fibroblasts) from day 2 to day 7. Comparing this data with the growth in diameter of the nodules in different conditions suggests a trend towards increased proliferation mediated by PSCs in PANC-1 nodules, although this was not significantly different from monocultures ($P>0.05$). There was no significant difference in the proliferation of the nodules +/− MRC5 cells.

A similar trend in increased proliferation was observed in CFPAC-1 cultures in the presence of PSCs, although this increase was also not significantly different from monocultures ($P>0.05$). Also, the number of CFPAC-1 nodules from day 2 to 7 +/− PSC was the same. The number of CFPAC-1 nodules decreased more in the presence of MRC5 cells compare to PSCs. However, the growth rate of CFPAC-1 nodules was lower than the nodules +/− PSC ($P>0.05$). Our result was consistent with a study on a 3D co-culture with GFP-labeled tumor-derived murine pancreatic organoids and PSCs (41). They showed that there was no significant difference between nodule proliferation +/− PSCs. However, there was a significant growth in PSCs proliferation in co-culture. Also, nodule size distributions at day 7 showed non-significant difference between the number of larger nodules ($\geq 6400 \mu m^2$) +/− fibroblasts, suggesting that there was no significant impact on nodule volume in these co-

cultures (Supplementary Figures S2A and S2B). A greater number of smaller objects when fibroblasts were available was due to visibility of fibroblasts themselves under the microscope. Our measurements were based on feature size in image data, not cell counts, and we had not attempted to quantify the number of fibroblastic cells embedded in the underlying matrix.

Heterocellular 3D co-cultures with stromal fibroblasts exhibit chemoresistance relative to homotypic 3D cultures

To examine the impact of co-culture conditions on chemosensitivity, we contrasted response to gemcitabine and oxaliplatin chemotherapies in PANC-1/fibroblast combination which were found in the characterization studies to exhibit strongest evidence of tumor-promoting stromal crosstalk. It has been established previously that paracrine crosstalk with PSCs in PDAC promotes cell survival through decreased apoptosis signaling (42). As expected, our data showed residual live nodule volume after treatment decreased in 3D cell cultures both with and without fibroblasts as the chemotherapy dose increased. Also, the presence of fibroblasts further diminished the response to oxaliplatin and gemcitabine chemotherapy. The effect was more dramatic with MRC5 than PSC cells (Figure 4A-D). An experiment on PDAC CAFs showed that different types of CAFs in PDAC had different chemosensitivity and that fibroblasts had an innate resistance to gemcitabine (43). Similarly, in our study both fibroblastic cell types, PSC and MRC5, showed minimal response to gemcitabine and oxaliplatin, and promoted chemoresistance in co-cultures. (Figure 4E).

PDT response is increased in 3D co-cultures with stromal fibroblasts

Following the same experimental design as the chemotherapy response studies, we also examined the impact of each PDAC/fibroblast co-culture condition on response to PDT using verteporfin. In direct contrast to the impact of fibroblast co-cultures on chemosensitivity, PDT response in PDAC cells (both PANC-1 and CFPAC-1) was enhanced when fibroblasts (MRC5 or PSCs) were present ($P<0.05$) (Figure 5A-D). This is a provocative result which goes against the prevailing trend that fibroblasts generally promote therapeutic resistance. As shown in Figure 5B and 5D which represent the dose response in CFPAC-1 ± fibroblasts, the difference between 10 J/cm^2 and 20 J/cm^2 was very small within the variability of the assay. Presumably with very high n-values there would be sufficient statistical power to resolve these differences in response even at intermediate PDT doses. In addition to enhanced response in PDAC cells, we also noted that the fibroblast populations themselves are highly sensitive to PDT and generally stain positive for ethidium bromide (cell death) even at intermediate PDT doses that produce only partial response in the tumor compartment of the co-cultures (Figure 5E). Moreover, Figure 5F shows the contrast between elongated fibroblasts surrounding cancer cells in the left panel versus dead fibroblasts surrounding the nodule in the right panel. This is in stark contrast to the chemotherapy response of fibroblasts noted above.

Another factor which could be considered to account for differences in PDT response is the uptake of verteporfin across cell culture conditions. However, while the verteporfin uptake and localization were not assessed for each cell culture scenario in this study, it does not seem likely that this could explain the trend toward increased cancer cell death in the

presence of fibroblasts. Since the co-cultures had a higher total cell number but the same total amount of verteporfin delivered, there could potentially be less available for uptake by either cell population. But if this were the case, we would expect to see decreased response to PDT, rather than the opposite effect.

Analysis of PDT-induced apoptotic and necrotic cell death in fibroblasts and co-cultures

To further examine PDT sensitivity in fibroblasts, we examined overall dose response as well as relative levels of early apoptosis in homotypic fibroblast monolayer cultures and in co-cultures. Overall dose response data for PDAC and fibroblasts in monolayer is shown in Figure 6A. The results show that both the PSC and MRC5 cells were highly sensitive to verteporfin PDT as compared to PANC-1 cells. As shown in Figure 6A, the fibroblasts (cultured on their own) are dramatically more sensitive to PDT than what is observed for either PDAC cell line in 3D culture. For example, at a light dose of 1J/cm^2, the viability of PSC and MRC5 cells normalized to no treatment control were 0.25 ± 0.04, 0.02 ± 0.01 respectively, as compared to 1.27 ± 0.03 for PANC-1 cells. The relatively high sensitivity of fibroblasts even at low light doses can also be seen in comparison with previously reported verteporfin PDT dose response for a larger panel of PDAC cell lines in monolayer culture (44). It is not surprising that normal cells were more susceptible to PDT-induced phototoxicity since resisting cell death is indeed a hallmark of cancer, and therapeutic index in PDT is achieved through selective light delivery and PS localization rather than intrinsic differential sensitivity to PDT in normal and cancer cells. It seems plausible that in PDAC tumors with fibrous stroma densely intermingled among pockets of cancer cells, that PDT dose will also be delivered to stromal cells as in these in vitro models. Hence the high sensitivity of stromal fibroblasts to PDT and subsequent consequences of photodestruction of this cell populations could be clinically relevant to PDT for PDAC.

As Figure 6B shows, apoptosis was dominant at lower light doses for verteporfin-PDT (which induces photodamage to mitochondria and endoplasmic reticulum) (45) (46) (47), while necrotic response was dominant at higher doses. This trend was more pronounced in MRC5 and PANC-1 cells compared to PSC cells (Figure 6B). The higher acute necrotic death of a large proportion of MRC5 cells compared to PSC potentially suggests a larger transient burst of cytokines into the microenvironment which could be related to the more dramatic impact on PDAC nodules in the MRC5 co-cultures. Further analysis of cytokine panels in PDT treated co-culture supernatants are needed to identify changes in levels of relevant cytokines following PDT treatment to identify which secreted cytokines are implicated in this.

Having found that cancer cell death generally increased in co-cultures, we sought to examine whether the increase in overall killing was predominantly apoptosis, necrosis, or a combination of both. To assess relative levels of apoptosis and necrosis we performed Annexin V and propidium iodide staining in 3D co-cultures of PANC-1, with and without fibroblasts (Figures 6C and 6D). These results showed that co-cultures generally exhibited an increase in both necrotic and apoptotic cell death without a convincing predominance of one or the other. This is observed in co-culture with both fibroblastic cell types (though the increase in apoptosis in the presence of PSC cells was not significant).

Conclusion

We investigated the impact of stromal fibroblasts on PDT and chemotherapy response in 3D co-cultures using fibroblasts which exhibit varying phenotypic traits. Our results showed that while co-culture with fibroblasts generally promoted chemoresistance, PDT response was enhanced when fibroblasts were present. Our data suggests the hypothesis that the increased killing of cancer cells may be caused by a bystander effect due to the acute necrotic death of a large proportion of fibroblasts and subsequent release of cytokines in the microenvironment. Similar stromal bystander effects have been observed with radiotherapy in other contexts (48). Here it was significant that the presence of fibroblasts in co-culture, which was found to promote increased chemoresistance, had the reverse effect on response to PDT. While both fibroblast cell types examined generally promoted the same trend toward decreased chemosensitivity and increased sensitivity to PDT, this effect was most pronounced with MRC5 co-cultured with PANC-1 cells. This observation however is consistent with the data presented in Figure 2 (high IL1-α, relatively low α-SMA) when taken in context of previous literature demonstrating tumor promoting and suppressing roles of the iCAF and myCAF phenotypes, respectively. Here we saw that co-culture conditions which gave rise to iCAF features were also the conditions in which we saw the most chemoresistance. This same co-culture condition benfited most from the photodestruction of fibroblasts. In other words, the condition in which we saw the most evidence of the fibroblasts playing a tumor-promoting role, we also saw the greatest benefit of depleting fibroblasts.

Overall however, the high sensitivity of the stromal compartment itself points to the potential of PDT as an adjuvant therapy for stromal depletion, not only priming the tumor for increased death response, as seen here, but also potentially enhanced permeability of the notoriously dense PDAC stroma to subsequent drug delivery.

Supplementary Material

Refer to Web version on PubMed Central for supplementary material.

Acknowledgments:

We gratefully acknowledge funding from the National Cancer Institute to the UMass Boston – Dana Farber/Harvard Cancer Center U54 Partnership (U54CA156734) which has supported this project. Additional support (to I.R.) was provided by NIH R00 CA175292, NIH UL1 TR002489 (through NC TraCS), and the UNC-NC State Joint BME Department Start-up Fund. We also thank Oracle and Collage of Science and Mathematics at UMass Boston for fellowship support to VK. We would also like to thank Jeffrey La for his assistance with microscopy and Mayra Teixeira for assistance in data acquisition.

References:

1. Kamisawa T, Wood LD, Itoi T, & Takaori K Pancreatic cancer. The Lancet, 388(10039), 73–85. 2016.
2. Ware MJ, Keshishian V, Law JJ, Ho JC, Favela CA, Rees P, … & Coarfa C Generation of an in vitro 3D PDAC stroma rich spheroid model. Biomaterials, 108, 129–142. 2016. [PubMed: 27627810]
3. Korc M Pancreatic cancer–associated stroma production. The American journal of surgery, 194(4), S84–S86. 2007. [PubMed: 17903452]

4. Rasheed ZA, Matsui W, & Maitra A Pathology of pancreatic stroma in PDAC. In Pancreatic cancer and tumor microenvironment. Transworld Research Network. 2012.
5. Procacci P, Moscheni C, Sartori P, Sommariva M, & Gagliano N Tumor–stroma cross-talk in human pancreatic ductal adenocarcinoma: A focus on the effect of the extracellular matrix on tumor cell phenotype and invasive potential. Cells, 7(10), 158. 2018.
6. Walker C, Mojares E, & del Río Hernández A Role of extracellular matrix in development and cancer progression. International journal of molecular sciences, 19(10), 3028. 2018.
7. Apte MV, Park S, Phillips PA, Santucci N, Goldstein D, Kumar RK, … & Keogh G Desmoplastic reaction in pancreatic cancer: role of pancreatic stellate cells. Pancreas, 29(3), 179–187. 2004. [PubMed: 15367883]
8. Biffi G, Oni TE, Spielman B, Hao Y, Elyada E, Park Y, … & Tuveson DA (2019). IL1-induced JAK/STAT signaling is antagonized by TGFβ to shape CAF heterogeneity in pancreatic ductal adenocarcinoma. Cancer discovery, 9(2), 282–301. 2019. [PubMed: 30366930]
9. Stylianopoulos T, Martin JD, Chauhan VP, Jain SR, Diop-Frimpong B, Bardeesy N, … & Munn LL Causes, consequences, and remedies for growth-induced solid stress in murine and human tumors. Proceedings of the National Academy of Sciences, 109(38), 15101–15108. 2012.
10. Leca J, Martinez S, Lac S, Nigri J, Secq V, Rubis M, … & Loncle C Cancer-associated fibroblast-derived annexin A6+ extracellular vesicles support pancreatic cancer aggressiveness. The Journal of clinical investigation, 126(11), 4140–4156. 2016. [PubMed: 27701147]
11. Hale MD, Hayden JD, & Grabsch HI Tumour-microenvironment interactions: role of tumour stroma and proteins produced by cancer-associated fibroblasts in chemotherapy response. Cellular oncology, 36(2), 95–112. 2013.
12. Martinez-Outschoorn UE, Goldberg AF, Lin Z, Ko YH, Flomenberg N, Wang C, … & Lisanti MP Anti-estrogen resistance in breast cancer is induced by the tumor microenvironment and can be overcome by inhibiting mitochondrial function in epithelial cancer cells. Cancer biology & therapy, 12(10), 924–938. 2011. [PubMed: 22041887]
13. Sun Y, Campisi J, Higano C, Beer TM, Porter P, Coleman I, … & Nelson PS Treatment-induced damage to the tumor microenvironment promotes prostate cancer therapy resistance through WNT16B. Nature medicine, 18(9), 1359. 2012.
14. Bailey JM, Swanson BJ, Hamada T, Eggers JP, Singh PK, Caffery T, … & Hollingsworth MA Sonic hedgehog promotes desmoplasia in pancreatic cancer. Clinical cancer research, 14(19), 5995–6004. 2008. [PubMed: 18829478]
15. Olive KP, Jacobetz MA, Davidson CJ, Gopinathan A, McIntyre D, Honess D, … & Frese KK Inhibition of Hedgehog signaling enhances delivery of chemotherapy in a mouse model of pancreatic cancer. Science, 324(5933), 1457–1461. 2009. [PubMed: 19460966]
16. Lee JJ, Perera RM, Wang H, Wu DC, Liu XS, Han S, … & Nagle JM Stromal response to Hedgehog signaling restrains pancreatic cancer progression. Proceedings of the National Academy of Sciences, 111(30), E3091–E3100. 2014.
17. Özdemir BC, Pentcheva-Hoang T, Carstens JL, Zheng X, Wu CC, Simpson TR, … & De Jesus-Acosta A Depletion of carcinoma-associated fibroblasts and fibrosis induces immunosuppression and accelerates pancreas cancer with reduced survival. Cancer cell, 25(6), 719–734. 2014. [PubMed: 24856586]
18. Mpekris F, Papageorgis P, Polydorou C, Voutouri C, Kalli M, Pirentis AP, & Stylianopoulos T Sonic-hedgehog pathway inhibition normalizes desmoplastic tumor microenvironment to improve chemo-and nanotherapy. Journal of Controlled Release, 261, 105–112. 2017. [PubMed: 28662901]
19. Dougherty TJ An update on photodynamic therapy applications. Journal of clinical laser medicine & surgery, 20(1), 3–7. 2002. [PubMed: 11902352]
20. Brown SB, Brown EA, & Walker I The present and future role of photodynamic therapy in cancer treatment. The lancet oncology, 5(8), 497–508. 2004. [PubMed: 15288239]
21. Huang Z, Xu H, Meyers AD, Musani AI, Wang L, Tagg R, … & Chen YK Photodynamic therapy for treatment of solid tumors—potential and technical challenges. Technology in cancer research & treatment, 7(4), 309–320. 2008. [PubMed: 18642969]

22. Sorrin AJ, Ruhi MK, Ferlic NA, Karimnia V, Polacheck WJ, Celli JP, … & Rizvi I Photodynamic Therapy and the Biophysics of the Tumor Microenvironment. Photochemistry and Photobiology. 2020.
23. Ayaru L, Bown SG, & Pereira SP Photodynamic therapy for pancreatic and biliary tract carcinoma. International journal of gastrointestinal cancer, 35(1), 1–13. 2005. [PubMed: 15722569]
24. Huggett MT, Jermyn M, Gillams A, Illing R, Mosse S, Novelli M, … & Pereira SP Phase I/II study of verteporfin photodynamic therapy in locally advanced pancreatic cancer. British journal of cancer, 110(7), 1698. 2014. [PubMed: 24569464]
25. DeWitt JM, Sandrasegaran K, O'Neil B, House MG, Zyromski NJ, Sehdev A, … & Shahda S Phase 1 study of EUS-guided photodynamic therapy for locally advanced pancreatic cancer. Gastrointestinal endoscopy, 89(2), 390–398. 2019. [PubMed: 30222972]
26. Rizvi I, Celli JP, Evans CL, Abu-Yousif AO, Muzikansky A, Pogue BW, … & Hasan T Synergistic enhancement of carboplatin efficacy with photodynamic therapy in a three-dimensional model for micrometastatic ovarian cancer. Cancer research, 70(22), 9319–9328. 2010 [PubMed: 21062986]
27. Anbil SR, Rizvi I, Celli JP, Alagic N, Pogue BW, & Hasan T Impact of treatment response metrics on photodynamic therapy planning and outcomes in a three-dimensional model of ovarian cancer. Journal of biomedical optics, 18(9), 098004. 2013. [PubMed: 24802230]
28. Zuluaga MF, & Lange N Combination of photodynamic therapy with anti-cancer agents. Current medicinal chemistry, 15(17), 1655–1673. 2008. [PubMed: 18673216]
29. Broekgaarden M, Rizvi I, Broekgaarden M, Rizvi I, Bulin AL, Petrovic L, Goldschmidt R, Massodi I, … & Hasan T, A. L, Petrovic L, Goldschmidt R, Massodi I, … & Hasan T Neoadjuvant photodynamic therapy augments immediate and prolonged oxaliplatin efficacy in metastatic pancreatic cancer organoids. Oncotarget, 9(16), 13009. 2018. [PubMed: 29560127]
30. Anbil S, Pigula M, Huang HC, Mallidi S, Broekgaarden M, Baglo Y, … & Rizvi I Vitamin D receptor activation and photodynamic priming enables durable low-dose chemotherapy. Molecular Cancer Therapeutics, 19(6), 1308–1319. 2020 : s.n. [PubMed: 32220968]
31. Celli JP Stromal interactions as regulators of tumor growth and therapeutic response: A potential target for photodynamic therapy?. Israel journal of chemistry, 52(8-9), 757–766. 2012. [PubMed: 23457416]
32. Lu J, Roy B, Anderson M, Leggett CL, Levy MJ, Pogue B, … & Wang KK Verteporfin-and sodium porfimer-mediated photodynamic therapy enhances pancreatic cancer cell death without activating stromal cells in the microenvironment. Journal of biomedical optics, 24(11), 118001. 2019.
33. Jones DP, Hanna W, Cramer GM, & Celli JP In situ measurement of ECM rheology and microheterogeneity in embedded and overlaid 3D pancreatic tumor stroma co-cultures via passive particle tracking. Journal of Innovative Optical Health Sciences, 10(06), 1742003. 2017.
34. Krempley BD, & Yu KH Preclinical models of pancreatic ductal adenocarcinoma. Chin Clin Oncol, 6(3), 25–25. 2017. [PubMed: 28705002]
35. Coleman SJ, Watt J, Arumugam P, Solaini L, Carapuca E, Ghallab M, … & Kocher HM Pancreatic cancer organotypics: High throughput, preclinical models for pharmacological agent evaluation. World journal of gastroenterology: WJG, 20(26), 8471. 2014. [PubMed: 25024603]
36. Collisson EA, Sadanandam A, Olson P, Gibb WJ, Truitt M, Gu S, … & Feiler HS Subtypes of pancreatic ductal adenocarcinoma and their differing responses to therapy. Nature medicine, 17(4), 500. 2011.
37. Lee GY, Kenny PA, Lee EH, & Bissell MJ Three-dimensional culture models of normal and malignant breast epithelial cells. Nature methods, 4(4), 359–365. 2007. [PubMed: 17396127]
38. Quantitative imaging reveals heterogeneous growth dynamics and treatment-dependent residual tumor distributions in a three-dimensional ovarian cancer model. Journal of biomedical optics, 15(5), 051603. Celli JP, Rizvi I, Evans CL, Abu-Yousif AO, & Hasan T 2010. [PubMed: 21054077]
39. An imaging-based platform for high-content, quantitative evaluation of therapeutic response in 3D tumour models. Scientific reports, 4, 3751. Celli JP, Rizvi I, Blanden AR, Massodi I, Glidden MD, Pogue BW, & Hasan T 2014. [PubMed: 24435043]

40. Somerville TD, Xu Y, Miyabayashi K, Tiriac H, Cleary CR, Maia-Silva D, … & Vakoc CR TP63-mediated enhancer reprogramming drives the squamous subtype of pancreatic ductal adenocarcinoma. Cell reports, 25(7), 1741–1755. 2018. [PubMed: 30428345]

41. Öhlund D, Handly-Santana A, Biffi G, Elyada E, Almeida AS, Ponz-Sarvise M, … & Chio IIC Distinct populations of inflammatory fibroblasts and myofibroblasts in pancreatic cancer. Journal of Experimental Medicine, 214(3), 579–596. 2017.

42. Vonlaufen A, Phillips PA, Xu Z, Goldstein D, Pirola RC, Wilson JS, & Apte MV (2008). Pancreatic stellate cells and pancreatic cancer cells: an unholy alliance. Cancer research, 68(19), 7707–7710. [PubMed: 18829522]

43. Richards KE, Zeleniak AE, Fishel ML, Wu J, Littlepage LE, & Hill R Cancer-associated fibroblast exosomes regulate survival and proliferation of pancreatic cancer cells. Oncogene, 36(13), 1770–1778. 2017. [PubMed: 27669441]

44. Celli JP, Solban N, Liang A, Pereira SP, & Hasan T Verteporfin-based photodynamic therapy overcomes gemcitabine insensitivity in a panel of pancreatic cancer cell lines. Lasers in surgery and medicine, 43(7), 565–574. 2011. [PubMed: 22057484]

45. Rizvi I, Obaid G, Bano S, Hasan T, & Kessel D (2018). Photodynamic therapy. Promoting in vitro efficacy of photodynamic therapy by liposomal formulations of a photosensitizing agent. Lasers in surgery and medicine, 50(5), 499–505. [PubMed: 29527710]

46. Rizvi I, Nath S, Obaid G, Ruhi MK, Moore K, Bano S, … & Hasan T A combination of visudyne and a lipid-anchored liposomal formulation of benzoporphyrin derivative enhances photodynamic therapy efficacy in a 3D model for ovarian cancer. Photochemistry and photobiology, 95(1), 419–429. 2019. [PubMed: 30499113]

47. Kessel D, & Reiners JJ Jr Enhanced efficacy of photodynamic therapy via a sequential targeting protocol. Photochemistry and photobiology, 90(4), 889–895. 2014. [PubMed: 24617972]

48. Marín A, Martín M, Liñán O, Alvarenga F, López M, Fernández L, … & Cerezo L (2015). Bystander effects and radiotherapy. Reports of Practical Oncology & Radiotherapy, 20(1), 12–21. [PubMed: 25535579]

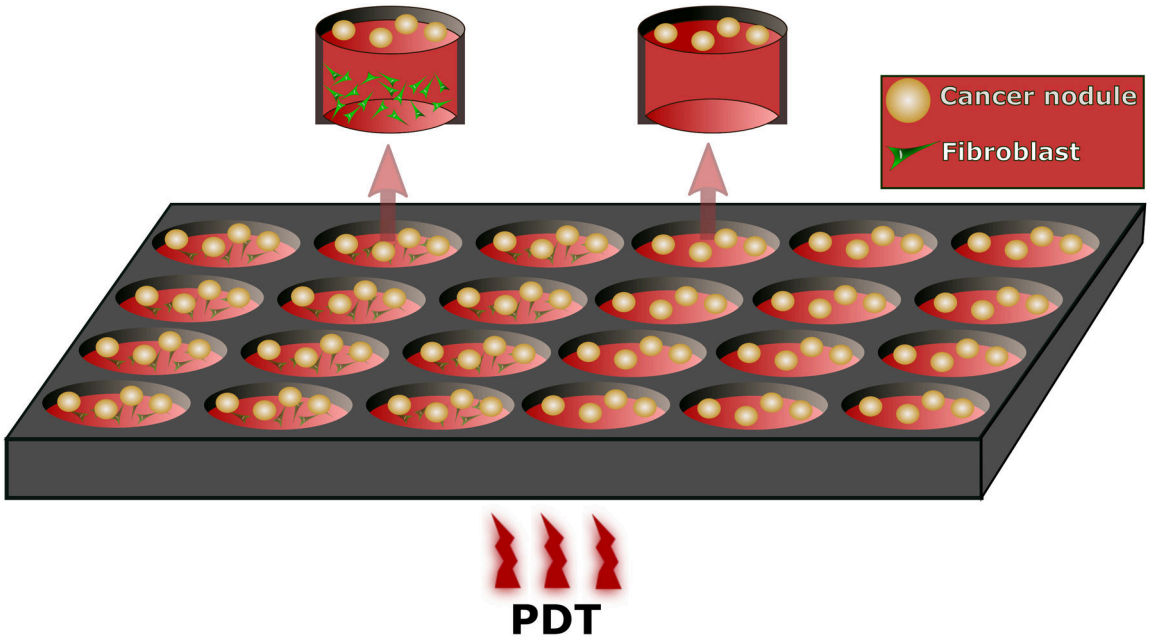

Figure 1.
Schematic diagram of PSCs or MRC5 co-cultured with PANC-1 or CFPAC-1 cells (3 left columns in the plate) and homo culture of the PANC-1 or CFPAC-1 cells (3 right columns).

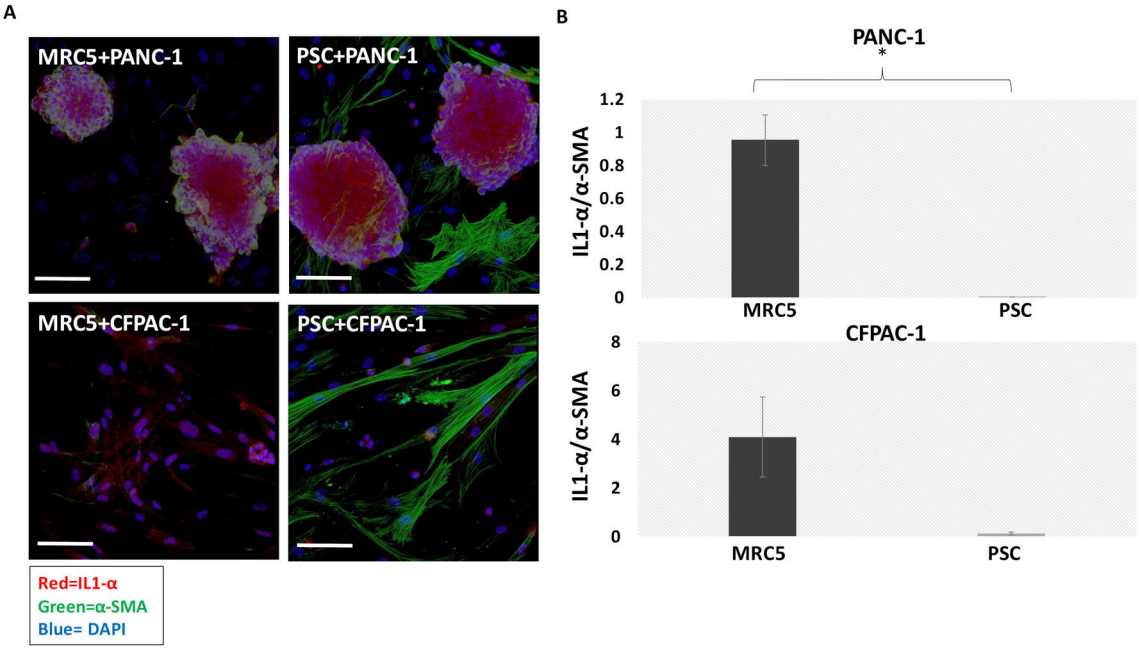

Figure 2.

A) 3D confocal images of fibroblasts co-cultured with PANC-1 or CFPAC-1 nodules. Red= IL1-α, green= α-SMA, blue=DAPI. Scale bar = 200μm B) Upper graph shows the IL1-α / α-SMA expressions in MRC5 and PCS cells co-cultured with PANC-1 nodules. Lower graph shows the IL1-α /α-SMA expressions in MRC5 and PCS cells co-cultured with CFPAC-1 nodules. Higher IL1-α /α-SMA expression in PSCs compared to MRC5 is observed in both co-culture types. Results were considered significant if $P < 0.05$ (*)

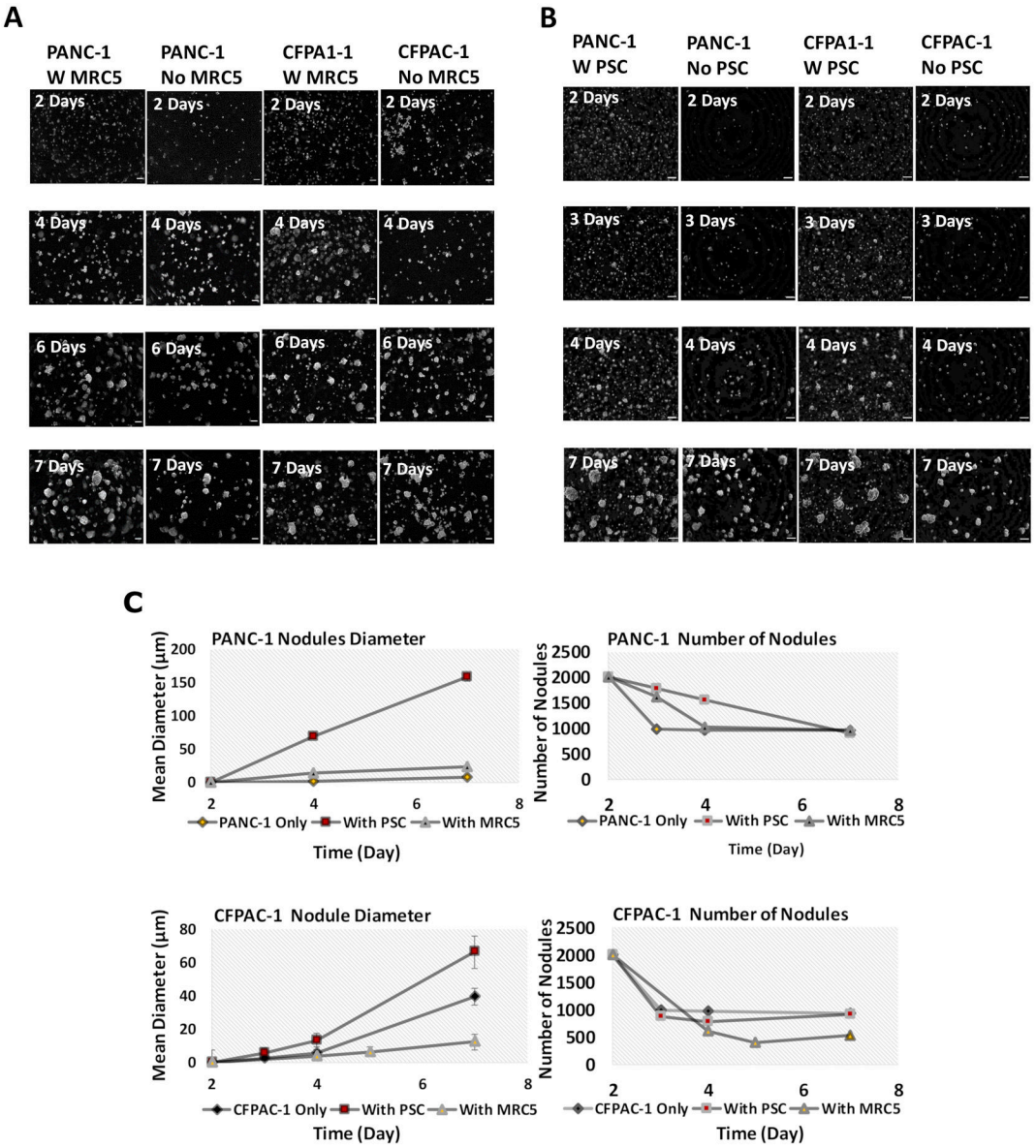

Figure 3.

Representative dark-field microscopy images of A) in vitro 3-D nodules +/− MRC5 B) in vitro 3-D nodules +/− PSC. Scale bar = 200µm C) representative mean diameter of the nodules (left) and the number of nodules per day (right). No significant difference in growth rate of nodules is observed (P>0.05).

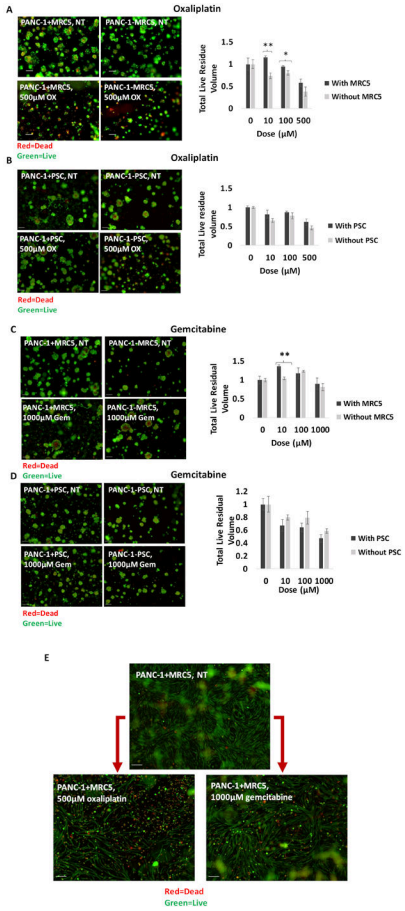

Figure 4.

Comparison between total live residual volume of PANC-1 nodules 48 hours after oxaliplatin treatment with (black) and without (gray) A) MRC5 cells. B) PSC cells. Comparison between total live residual volume of PANC-1 nodules 48 hours after gemcitabine treatment with (black) and without (gray) C) MRC5 cells. D) PSC cells. The live residual volume decreased as the chemotherapy dose increased. Also, the presence of fibroblasts further diminished the response to chemotherapy. Results were considered significant if $P < 0.05$ (*), $P < 0.01$ (**). E) The comparison between the effect of chemotherapy on fibroblasts using lower focal plane images. The fibroblasts exhibited minimal response to gemcitabine and oxaliplatin even at the highest doses used in this experiment.

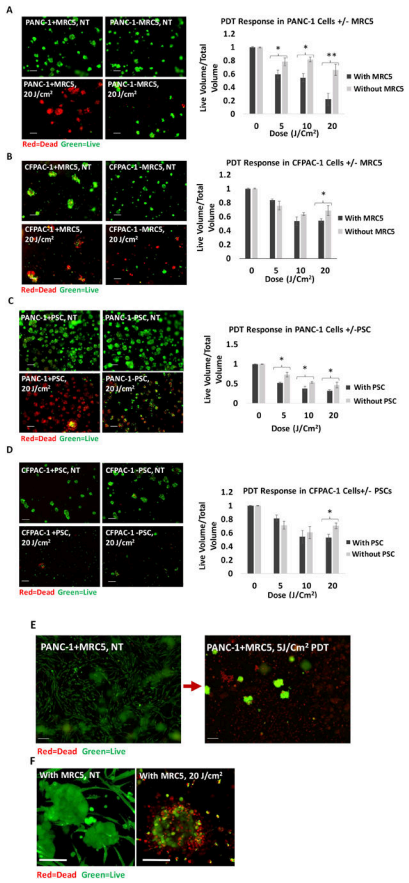

Figure 5.

Comparison between PDT response in A) PANC-1 cells with (black) and without (gray) MRC5. B) CFPAC-1 cells with (black) and without (gray) MRC5s. C) PANC-1 cells with (black) and without (gray) PSCs. D) CFPAC-1 cells with (black) and without (gray) PSCs. In all situations, the PDT response is increased in co-cultures in the presence of fibroblasts. Results were considered significant if $P < 0.05$ (*), $P < 0.01$ (**). E) Fibroblasts exhibit dramatic response to PDT with complete cell death at 5J/cm^2 PDT. There is significant residual 3D tumor volume at the same dose (green). F) The contrast between elongated fibroblasts surrounding cancer cells in the left panel versus dead fibroblasts surrounding the nodule in the right panel. Scale bars = 200 μm.

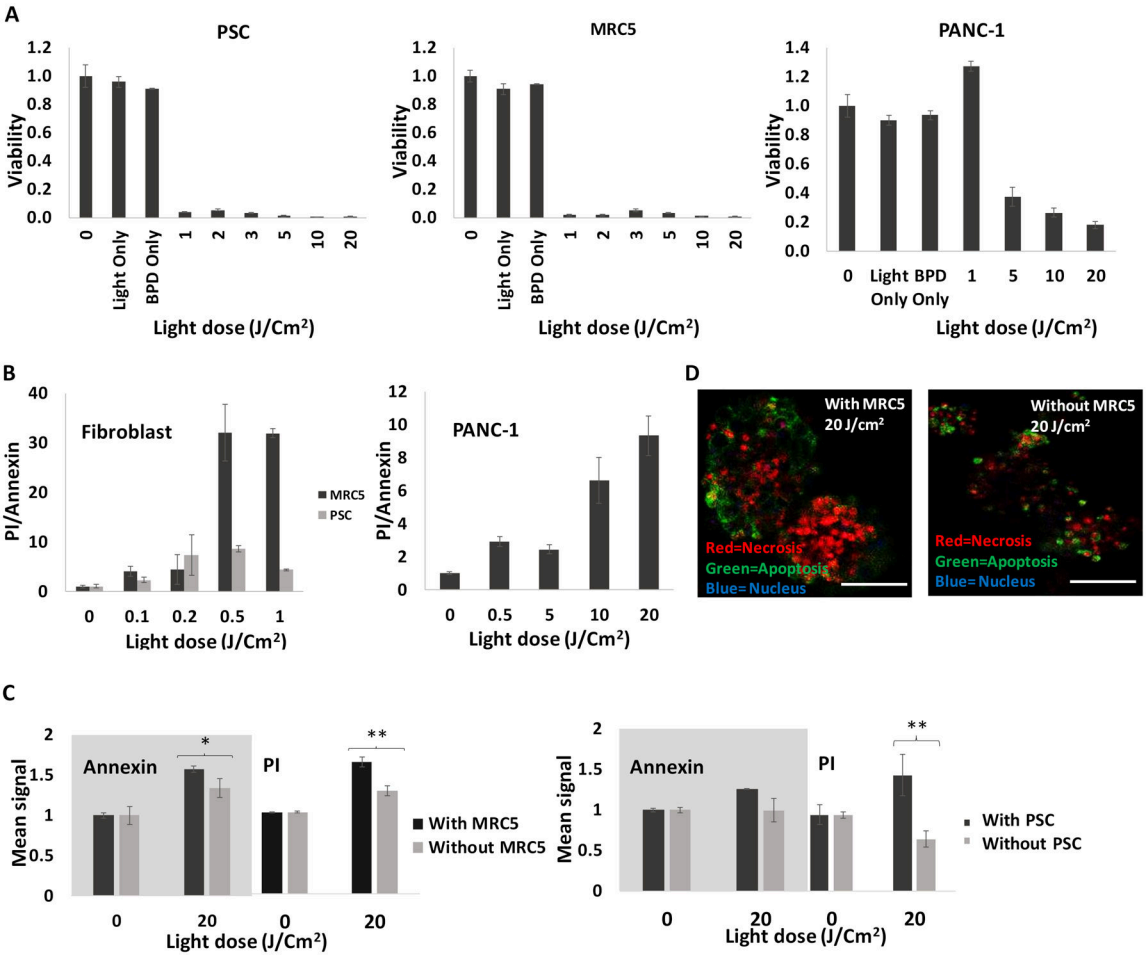

Figure 6.

A) PDT dose response in fibroblasts and PANC-1 cells. Fibroblasts are highly sensitive to veteporfin PDT compare to PANC-1. B) Ratio of PI to Annexin V, 3 hours post PDT (PI=necrotic, annexin=apoptotic) for fibroblasts and PANC-1 cells in monolayer. As ratio increases, there's more necrosis, and C) Comparison between apoptosis and necrosis 3 hours post PDT for PANC-1 cells +/− fibroblasts. Higher necrotic and apoptotic cell death is observed in the presence of fibroblasts. Results were considered significant if $P < 0.05$ (*), $P< 0.01$ (**). D) Confocal images of PANC-1 cells +/− fibroblasts 3 hours after 20J/Cm^2 PDT. Scale bars = 200μm.